Prospects for dark matter signal discovery and model selection via timing information in a low-threshold experiment

Journal of Cosmology and Astroparticle Physics

SISSA

PAPER • OPEN ACCESS

Prospects for dark matter signal discovery and model selection via timing information in a low-threshold experiment

To cite this article: Riccardo Catena and Vanessa Zema JCAP02(2022)022

Journal of Cosmology and Astroparticle Physics
An IOP and SISSA journal

Prospects for dark matter signal discovery and model selection via timing information in a low-threshold experiment

Riccardo Catena[a] **and Vanessa Zema**[a,b,c]

[a]Chalmers University of Technology, Department of Physics, SE-412 96, Göteborg, Sweden
[b]GSSI-Gran Sasso Science Institute, 67100, L'Aquila, Italy
[c]Max Planck Institute for Physics, 80805, Munich, Germany

E-mail: catena@chalmers.se, vanezema@mpp.mpg.de

Received November 15, 2021
Accepted January 12, 2022
Published February 14, 2022

Abstract. In the recent years, many low-threshold dark matter (DM) direct detection experiments have reported the observation of unexplained excesses of events at low energies. Exemplary for these, the experiment CRESST has detected unidentified events below an energy of about 200 eV — a result hampering the detector performance in the search for GeV-scale DM. In this work, we test the impact of nuclear recoil timing information on the potential for DM signal discovery and model selection on a low-threshold experiment limited by the presence of an unidentified background resembling this population of low-energy events. Among the different targets explored by the CRESST collaboration, here we focus on Al_2O_3, as a sapphire detector was shown to reach an energy threshold as low as 19.7 eV [1]. We test the ability of a low-threshold experiment to discover a signal above a given background, or to reject the spin-independent interaction in favour of a magnetic dipole coupling in terms of p-values. We perform our p-value calculations: 1) taking timing information into account; and 2) assuming that the latter is not available. By comparing the two approaches, we find that under our assumptions timing information has a marginal impact on the potential for DM signal discovery, while provides more significant results for the selection between the two models considered. For the model parameters explored here, we find that the p-value for rejecting spin-independent interactions in favour of a magnetic dipole coupling is about 0.11 when the experimental exposure is 460 g×year and smaller (about 0.06) if timing information is available. The conclusion on the role of timing information remains qualitatively unchanged for exposures as large as 1 kg×5 year. At the same time, our results show that a 90% C.L. rejection of spin-independent interactions in favour of a magnetic dipole coupling is within reach of an upgrade of the CRESST experiment [2].

Keywords: dark matter experiments, dark matter theory

ArXiv ePrint: 2110.15826

https://doi.org/10.1088/1475-7516/2022/02/022

JCAP02(2022)022

Contents

1 Introduction

While the identity of our Universe's invisible mass component, Dark Matter (DM), remains unknown, the experimental search for its microscopic constituents progressed rapidly in recent years [3]. In particular, the search for nuclear recoils induced by the non-relativistic scattering of Milky Way DM particles in low-background deep underground detectors — the so-called DM direct detection technique [4, 5] — played, and will continue playing, a central role in this context [6]. For example, the null result of the operating experiments led to stringent constraints on the DM-nucleon and -electron coupling, e.g. [7], and the effort placed on assessing the expected performance of next-generation direct detection experiments has been remarkable in recent years [8–15]. In this assessment, the performance of an experiment is measured by the exposure it must reach to reject the background-only hypothesis for a specific background model, or to reject a particle physics model in favour of an alternative one at a given significance. This assessment is crucial, as it contributes determining which experiments to prioritise in the coming years. One important component of this assessment is to clarify quantitatively whether the simultaneous measurement of nuclear recoil energy spectrum and associated time distribution of the observed recoils is advantageous for a given experimental setup, or it is preferable to focus on the measurement of the energy spectrum alone. This question must be addressed proactively, as building ultra-low background experiments that are stable over the time scale of one year (the period of the Earth revolution around the Sun) is a difficult experimental approach posing highly non trivial challenges in particular for cryogenic detectors.

JCAP02(2022)022

The impact of timing information on the ability of direct detection experiments to distinguish DM models with nearly degenerate recoil spectra has been investigated for single-target experiments employing fluorine, germanium or xenon targets and with a relatively high energy threshold in [16]. Using a Bayesian approach to model selection, ref. [16] finds that including timing information may enhance this ability, but only with exposures beyond the expectation of the experiments currently running (indicated as Generation 2 experiment in [16]). The results of ref. [16] apply to weakly interacting massive particles of mass around 50 GeV and cannot a priori be extended to DM at the GeV scale. This extension would require lowering the assumed energy threshold below about 0.3 keV.

Similarly, the impact of timing information on the ability of direct detection experiments to identify a DM signal over an experimental background has not been investigated for low-threshold experiments. Consequently, it remains unclear whether it is worth taking the challenge of operating cryogenic experiments under stable conditions over a period of one year or longer. Importantly, this is a timely question, as the low-threshold experiment CRESST has recently reported unexplained low-energy events in one of the detector modules [17]. These start at the detector energy threshold, 30.1 eV, and extend up to 200 eV, inside the acceptance region in the light yield - recoil energy plane. The CRESST collaboration reports that the excess is present in all the operated modules and that its energy distribution varies from module to module, observation which disfavours a single common origin of this effect. However, this excess limits CRESST sensitivity. Consequently, it is reasonable to ask whether a time-dependent analysis improves the significance for signal identification and model selection in the presence of such background. In this work, we investigate the impact of timing information on the potential for DM signal discovery and model selection of a low-threshold experiment. The analysis is divided into two parts. In the first one, we test the impact of timing information on the ability of a low-threshold experiment to discover a DM signal over an experimental background that resembles the population of low-energy events found in [17]. The second part of the analysis focuses on DM model selection. Here, we test the ability of a low-threshold experiment to reject a model where DM couples to nucleons via spin-independent interactions in favour of an alternative hypothesis where DM couples to nuclei via magnetic dipole interactions. Our choice of alternative hypothesis is motivated by the fact that the time of maximum DM-induced nuclear recoil rate as a function of the minimum velocity required to transfer a given momentum in the scattering can be target-dependent in the case of magnetic dipole interactions, whereas it does not depend on the target for spin-independent interactions [18]. Consequently, a multi-target experiment like CRESST should be able to exploit this feature when comparing different DM models. Remarkably, we find that timing information has not a significant impact on DM signal discovery, but on model selection for experimental exposures that are within reach of next-generation, low-threshold direct detection experiments. For example, we find that with an exposure of 460 g$\times$year the p-value for rejecting spin-independent interactions in favour of a magnetic dipole coupling is around 0.11, while it is about 0.06 when the time distribution of the event rate is available. At the same time, our results show that a 90% C.L. rejection of spin-independent interactions is within reach of a future upgrade of the CRESST experiment [2].

This work is organised as follows. In section 2 we outline the theoretical framework used in our analysis. In section 3, we critically review the timing information that is available to a low-threshold, multi-target experiment like CRESST. In section 4, we introduce the statistical framework that we apply to assess the prospects for DM signal discover and model selection with a low-threshold experiment. We present our results on DM signal discovery in section 5.1

JCAP02(2022)022

and on DM model selection in section 5.2. We finally summarise and conclude in section 6. In an appendix, we list useful expressions to compute scattering rates and cross sections in the case of spin 1/2 DM.

2 Theoretical framework

The differential rate of DM-nucleus scattering events per unit detector mass in a direct detection experiment can be expressed as an integral over DM particle velocities in the detector rest frame,

$$\frac{\mathrm{d}R}{\mathrm{d}E_R} = \sum_T \xi_T \frac{\rho_\chi}{m_\chi m_T} \int_{|\boldsymbol{v}|\geq v_{\min}} \mathrm{d}^3 v \, |\boldsymbol{v}| f(\boldsymbol{v}, t) \, \frac{\mathrm{d}\sigma_T}{\mathrm{d}E_R} \,, \tag{2.1}$$

where $v_{\min} = \sqrt{2 m_T E_R}/(2\mu_T)$ is the minimum velocity a DM particle must have to deposit an energy E_R in the detector, m_T and μ_T are the target nucleus and DM-nucleus reduced mass, respectively, m_χ is the DM particle mass and ρ_χ is the local DM density. In multi-target detectors, like CRESST, the contribution to eq. (2.1) of each element in the detector material is weighted by the corresponding mass fraction, ξ_T. The differential rate of DM-nucleus scattering events also depends on the differential cross section for DM-target nucleus scattering, $\mathrm{d}\sigma_T/\mathrm{d}E_R$, and on the local DM velocity distribution expressed as a function of the DM velocity in the detector reference frame, $f(\boldsymbol{v}, t)$. The velocity distribution $f(\boldsymbol{v}, t)$ is a periodic function of time, t, with period of one year. As a result, the expected rate of nuclear recoils is a function of time with the same periodicity. We model $f(\boldsymbol{v}, t)$ by taking the gravitational focusing of the Sun into account, which implies [19],

$$f(\boldsymbol{v}, t) = \tilde{f}(\boldsymbol{v}_\odot + \boldsymbol{v}_\infty[\boldsymbol{v} + \boldsymbol{V}_\oplus(t)]) \,, \tag{2.2}$$

where $\tilde{f}$ is the DM velocity distribution in the Galactic reference frame (where, by construction, the mean velocity of DM particles is zero), $\boldsymbol{v}_\odot \simeq (11, 232, 7)$ km s^{-1} is the relative velocity of the Sun with respect to the Galactic centre in Galactic coordinates, $\boldsymbol{v}$ is the DM particle velocity in the detector rest frame and $\boldsymbol{V}_\oplus(t)$ is the relative velocity of the Earth with respect to the Sun. Consistently, we denote by $\boldsymbol{v_s} = \boldsymbol{v} + \boldsymbol{V}_\oplus$ the DM particle velocity in the Sun rest frame. With this notation, the solar frame velocity $\boldsymbol{v}_\infty$ a DM particle must have at infinity to move with velocity $\boldsymbol{v_s}$ with respect to the Sun at the detector position is given by [19],

$$\boldsymbol{v}_\infty[\boldsymbol{v_s}] = \frac{v_\infty^2 \boldsymbol{v_s} + v_\infty (GM_\odot/r_s)\hat{\boldsymbol{r}}_\boldsymbol{s} - v_\infty \boldsymbol{v_s}(\boldsymbol{v_s}\cdot\hat{\boldsymbol{r}}_\boldsymbol{s})}{v_\infty^2 + (GM_\odot/r_s) - v_\infty(\boldsymbol{v_s}\cdot\hat{\boldsymbol{r}}_\boldsymbol{s})} \,, \tag{2.3}$$

where r_s is Earth-Sun distance, $\hat{\boldsymbol{r}}_\boldsymbol{s}$ is the time dependent unit vector that points from the Sun to the Earth, $v_\infty^2 = v^2 - 2GM_\odot/r_s$, $M_\odot$ is the mass of the Sun, and G is Newton's constant. Explicit expressions for $\boldsymbol{V}_\oplus$ and $\hat{\boldsymbol{r}}_\boldsymbol{s}$ in Galactic coordinates can be found in [20] and [21, 22], respectively. For $\tilde{f}$, we assume a Gaussian distribution truncated at the escape velocity $v_{\rm esc}$,

$$\tilde{f}(\tilde{\boldsymbol{v}}) = \frac{1}{N_{\rm esc}(2\pi\sigma_v^2)^{3/2}} \exp\left(-\frac{|\tilde{\boldsymbol{v}}|^2}{2\sigma_v^2}\right) \Theta\left(v_{\rm esc} - |\tilde{\boldsymbol{v}}|\right) \,, \tag{2.4}$$

where $\tilde{\boldsymbol{v}} = \boldsymbol{v}_\odot + \boldsymbol{v}_\infty$. Here, we assume the one-dimensional velocity dispersion $\sigma_v = 164$ km s^{-1} and a local escape velocity of $v_{\rm esc}, = 544$ km s^{-1}. The normalisation factor, $N_{\rm esc}$, in eq. (2.4) is given by,

$$N_{\rm esc} = \mathrm{erf}\left(\frac{v_{\rm esc}}{\sqrt{2}\sigma_v}\right) - \sqrt{\frac{2}{\pi}}\frac{v_{\rm esc}}{\sigma_v} \exp\left(-\frac{v_{\rm esc}^2}{2\sigma_v^2}\right) \,. \tag{2.5}$$

JCAP02(2022)022

$\mathcal{O}_1 = \mathbb{1}_{\chi N}$	$\mathcal{O}_9 = i\mathbf{S}_\chi \cdot \left(\mathbf{S}_N \times \frac{\mathbf{q}}{m_N}\right)$
$\mathcal{O}_3 = i\mathbf{S}_N \cdot \left(\frac{\mathbf{q}}{m_N} \times \mathbf{v}^\perp\right)$	$\mathcal{O}_{10} = i\mathbf{S}_N \cdot \frac{\mathbf{q}}{m_N}$
$\mathcal{O}_4 = \mathbf{S}_\chi \cdot \mathbf{S}_N$	$\mathcal{O}_{11} = i\mathbf{S}_\chi \cdot \frac{\mathbf{q}}{m_N}$
$\mathcal{O}_5 = i\mathbf{S}_\chi \cdot \left(\frac{\mathbf{q}}{m_N} \times \mathbf{v}^\perp\right)$	$\mathcal{O}_{12} = \mathbf{S}_\chi \cdot \left(\mathbf{S}_N \times \mathbf{v}^\perp\right)$
$\mathcal{O}_6 = \left(\mathbf{S}_\chi \cdot \frac{\mathbf{q}}{m_N}\right)\left(\mathbf{S}_N \cdot \frac{\hat{\mathbf{q}}}{m_N}\right)$	$\mathcal{O}_{13} = i\left(\mathbf{S}_\chi \cdot \mathbf{v}^\perp\right)\left(\mathbf{S}_N \cdot \frac{\mathbf{q}}{m_N}\right)$
$\mathcal{O}_7 = \mathbf{S}_N \cdot \mathbf{v}^\perp$	$\mathcal{O}_{14} = i\left(\mathbf{S}_\chi \cdot \frac{\mathbf{q}}{m_N}\right)\left(\mathbf{S}_N \cdot \mathbf{v}^\perp\right)$
$\mathcal{O}_8 = \mathbf{S}_\chi \cdot \mathbf{v}^\perp$	$\mathcal{O}_{15} = -\left(\mathbf{S}_\chi \cdot \frac{\mathbf{q}}{m_N}\right)\left[\left(\mathbf{S}_N \times \mathbf{v}^\perp\right) \cdot \frac{\mathbf{q}}{m_N}\right]$

Table 1. Interaction operators defining the non-relativistic effective theory of spin 1/2 DM-nucleon interactions [23, 24]. $\mathbf{S}_N$ ($\mathbf{S}_\chi$) is the nucleon (DM) spin, $\mathbf{v}^\perp = \mathbf{v} - \mathbf{q}/(2\mu_N)$, where μ_N is the DM-nucleon reduced mass, is the transverse relative velocity and $\mathbb{1}_{\chi N}$ is the identity in the DM-nucleon spin space.

The differential cross section for DM-nucleus scattering, $\mathrm{d}\sigma_T/\mathrm{d}E_R$ encodes all particle and nuclear physics inputs required to evaluate eq. (2.1). Within the non relativistic effective theory of DM-nucleon interactions, $\mathrm{d}\sigma_T/\mathrm{d}E_R$ can be expressed as follows,

$$\frac{\mathrm{d}\sigma_T}{\mathrm{d}E_R} = \frac{2m_T}{(2J_T+1)v^2} \sum_k \sum_{\tau,\tau'} \left(\frac{q^2}{m_N^2}\right)^{\ell_k} R_k^{\tau\tau'}\left(v_T^{\perp 2}, \frac{q^2}{m_N^2}\right) W_k^{\tau\tau'}(q^2)\,, \tag{2.6}$$

where J_T is the target nucleus spin, $v = |\mathbf{v}|$, $v_T^{\perp 2} = v^2 - q^2/(4\mu_T^2)$, $q = \sqrt{2m_T E_R}$ is the momentum transfer and m_N is the nucleon mass. At most eight DM and nuclear response functions, $R_k^{\tau\tau'}$ and $W_k^{\tau\tau'}$, $k = M, \Sigma', \Sigma'', \Phi'', \Phi''M, \tilde{\Phi}', \Delta, \Delta\Sigma'$, respectively, can appear in eq. (2.6) [24]. The $R_k^{\tau\tau'}$ functions depend on q^2/m_N^2, $v_T^{\perp 2}$ and on the coupling constants for DM-nucleon interactions, c_j^τ. They are known analytically, and we list them for spin 1/2 DM in the appendix. Here, the index j labels the type of DM-nucleon interaction [24]. Assuming one-body DM-nucleon interactions, there are $4 + 20J_\chi$ interaction types that are invariant under Galilean transformations and spatial rotations for a DM particle of spin J_χ [25]. We list the 14 independent interaction operators arising for spin 1/2 DM in table 1. The eight nuclear response functions $W_k^{\tau\tau'}$ in eq. (2.6) are quadratic in reduced matrix elements of nuclear charges and currents, and must be computed numerically. This calculation is performed within the nuclear shell model for heavy targets, such as xenon. However, for light nuclei *ab initio* methods have recently been applied [26]. The indexes τ and τ' run from 0 to 1: 0 corresponds to "isoscalar" interactions and 1 to "isovector" interactions [24]. In terms of, e.g. c_1^τ, the neutron to proton coupling ratio can be expressed as $r = c_p/c_n = (c_1^0 - c_1^1)/(c_1^0 + c_1^1)$. Finally, $\ell_k = 0$ for $k = M, \Sigma', \Sigma''$, and $\ell_k = 1$ otherwise.

The way the cross section $\mathrm{d}\sigma_T/\mathrm{d}E_R$ depends on v determines how the nuclear recoil rate depends on t. Inspection of eq. (A.1) shows that there are four ways the velocity v can enter the cross section $\mathrm{d}\sigma_T/\mathrm{d}E_R$. The interactions labelled by $\mathcal{O}_1$, $\mathcal{O}_7$, $\mathcal{O}_8$ and $\mathcal{O}_{11}$ in the literature [24] and here associated with the coupling constants c_1^τ, c_7^τ, c_8^τ and c_{11}^τ are representative of these four classes. The corresponding DM-nucleus scattering cross section

JCAP02(2022)022

reads as,

$$
\begin{aligned}
\left.\frac{\mathrm{d}\sigma_T}{\mathrm{d}E_R}\right|_{\mathcal{O}_1} &= \frac{2m_T}{(2J_T+1)v^2}\sum_{\tau\tau'} c_1^\tau c_1^{\tau'} W_M^{\tau\tau'}(q^2) \equiv \frac{a(q^2)}{v^2}\,, \\
\left.\frac{\mathrm{d}\sigma_T}{\mathrm{d}E_R}\right|_{\mathcal{O}_7} &= \frac{2m_T}{(2J_T+1)v^2}\sum_{\tau\tau'} c_7^\tau c_7^{\tau'} \frac{(v^2-v_{\mathrm{min}}^2)}{8} W_M^{\tau\tau'}(q^2) \equiv b(q^2)\left(1-\frac{v_{\mathrm{min}}^2}{v^2}\right)\,, \\
\left.\frac{\mathrm{d}\sigma_T}{\mathrm{d}E_R}\right|_{\mathcal{O}_8} &= \frac{2m_T}{(2J_T+1)v^2}\sum_{\tau\tau'} \frac{c_8^\tau c_8^{\tau'}}{4}\left[v^2 W_M^{\tau\tau'}(q^2) - v_{\mathrm{min}}^2\left(W_M^{\tau\tau'}(q^2) - 4\frac{\mu_T^2}{m_N^2} W_\Delta^{\tau\tau'}(q^2)\right)\right]\,, \\
&\equiv c(q^2)\left(1-\frac{v_{\mathrm{min}}^2}{v^2}\right) + d(q^2)\frac{v_{\mathrm{min}}^2}{v^2} \\
\left.\frac{\mathrm{d}\sigma_T}{\mathrm{d}E_R}\right|_{\mathcal{O}_{11}} &= \frac{2m_T}{(2J_T+1)v^2}\sum_{\tau\tau'} \frac{c_{11}^\tau c_{11}^{\tau'}}{4}\frac{q^2}{m_N^2} W_M^{\tau\tau'}(q^2) \equiv e(q^2)\frac{v_{\mathrm{min}}^2}{v^2}\,,
\end{aligned}
\tag{2.7}
$$

where we assumed that the DM particle has spin $J_\chi = 1/2$. In eq. (2.7), we also emphasised the dependence on v by introducing the functions a, b, c, d, and e which are implicitly defined via the above equation. We refer to [23, 24] for further details on the effective theory of DM-nucleon interactions and to [27, 28] for a discussion on its limitations and extensions. Here, we just mention that the $\mathcal{O}_1$ interaction is the familiar spin-independent interaction [24] and that the interactions $\mathcal{O}_7$, $\mathcal{O}_8$ and $\mathcal{O}_{11}$ arise from the non-relativistic reduction of simplified models. They can be the leading DM-nucleon interactions in specific ranges for the DM mass [29–32].

While in the non-relativistic effective theory of DM-nucleon interactions the coupling constants c_j^τ are considered as independent, in concrete models one generically expects to generate specific combinations of operators in table 1. In particular, this applies to the DM magnetic dipole model. The model assumes that DM is made of spin 1/2 particles and is characterised by the interaction Lagrangian $\mathscr{L} = \frac{1}{2}\lambda_\chi \overline{\chi}\sigma^{\mu\nu}\chi F_{\mu\nu}$, where χ is the DM spinor and $F_{\mu\nu}$ the electromagnetic field strength tensor. Here, the coupling constant λ_χ has dimension GeV^{-1}. From this Lagrangian one finds the non-relativistic amplitude for DM-nucleon scattering [33],

$$
\mathcal{M} = e\lambda_\chi\left[2m_N Q_N\langle\mathcal{O}_1\rangle + 4m_\chi g_N\langle\mathcal{O}_4\rangle + \frac{8m_N^2 m_\chi Q_N}{|\mathbf{q}|^2}\langle\mathcal{O}_5\rangle - \frac{4m_N^2 m_\chi g_N}{|\mathbf{q}|^2}\langle\mathcal{O}_6\rangle\right]\,, \tag{2.8}
$$

where Q_N, $N = p, n$, is the nucleon electric charge (0 for neutrons and 1 for protons), g_N, $N = p, n$, is the nucleon g-factor, and angle brackets denote matrix elements between two-component nucleon and DM spinors. Eq. (2.8) shows that the amplitude for DM-nucleon scattering in the DM magnetic dipole model is a linear combination of matrix elements of the operators in table 1 where some of the coefficients are constant while others scale like $1/|\mathbf{q}|^2$ with the momentum transfer. Consequently, if one promotes the coupling constants c_j^τ to functions of the momentum transfer, the DM magnetic dipole model arises from a specific combination of operators in table 1. The associated cross section for DM-nucleus scattering

JCAP02(2022)022

reads as follows,

$$\frac{\mathrm{d}\sigma_T}{\mathrm{d}E_R} = \frac{8m_T}{(2J_T+1)v^2}\alpha\pi\lambda_\chi^2\left[\left(\frac{1}{m_\chi^2}-\frac{1}{\mu_T^2}+\frac{1}{\mu_T^2}\frac{v^2}{v_{\rm min}^2}\right)W_M^{pp}+\frac{1}{m_N^2}\left(\tilde{\mu}_p^2 W_{\Sigma'}^{pp}+2\tilde{\mu}_p\tilde{\mu}_n W_{\Sigma'}^{np}\right.\right. \tag{2.9}$$
$$\left.\left.+\,\tilde{\mu}_n^2 W_{\Sigma'}^{nn}\right)+4W_\Delta^{pp}-4\tilde{\mu}_p W_{\Delta\Sigma'}^{pp}-4\tilde{\mu}_n W_{\Delta\Sigma'}^{pn}\right],$$

where α is the fine structure constant, while $\tilde{\mu}_N = g_N/2$, with $\tilde{\mu}_p = 2.8$ and $\tilde{\mu}_n = -1.9$, is the dimensionless magnetic moment of the nucleon [34]. The nuclear response functions in eq. (2.9) are related to the ones in eq. (2.7) by $W_M^{pp} = W_M^{00} + 2W_M^{01} + W_M^{11}$ and analogous expressions [24]. We conclude this section by specifying our choices of nuclear targets and response functions. So far, the CRESST experiment has exploited $CaWO_4$, Li_2MoO_4 and Al_2O_3 targets. Here, we primarily focus on detectors employing Al_2O_3 crystals. This choice is motivated by the fact that Al_2O_3 is made of two light elements, aluminium and oxygen, and Al_2O_3 detectors can operate with energy thresholds as low as 19 eV [1]. Both properties make Al_2O_3 a promising target to search for light DM particles of mass of a few GeV. Furthermore, aluminium has spin 5/2 and the corresponding $W_{\Sigma'}^{\tau\tau'}$, $W_\Delta^{\tau\tau'}$ and $W_{\Delta\Sigma'}^{\tau\tau'}$ functions are different from zero. Consequently, Al_2O_3 detectors can be used to probe a wide range of DM-nucleon interactions. In the calculations reported in section 3.1, section 3.2 and section 3.3, as well as in sections 5.1 and 5.2, we use the nuclear form factors of [35] for aluminium and oxygen (as well as calcium in some investigations). For the same elements, we use Helm form factors when treating the background amplitude as a nuisance parameter (see section 4), as they are faster to evaluate. Results obtained by using Helm form factors lead to overestimate the expected number of DM-induced nuclear recoil events by about 10%. Finally, when comparing the timing information available to a Al_2O_3 multi-target experiment with the one accessible with a fluorine, germanium, iodine, or xenon detector, for the latter we use the nuclear form factors provided by the `DMFormFactor` code [36].

3 Timing information in multi-target detectors

In this section, we critically review the timing information that is available to low-threshold multi-target DM direct detection experiments when DM couples to nuclei via one of the interactions in table 1. This timing information is contained in the coefficients of the Fourier series expansion of the differential rate of nuclear recoil events in eq. (2.1). The time-averaged rate, A_0, and the annual modulation amplitude, A_1, are the first two coefficients in this expansion. Starting from this observation, in section 3.1 we characterise the interactions in table 1 in terms of the predicted $A_1(v_{\rm min})$ curve. In section 3.2, we show that most of the timing information is contained in A_0 and A_1 for all interactions in table 1, and hence higher-order harmonics can be neglected. Finally, in section 3.3, we characterise the interactions in table 1 in terms of the predicted $t_{\rm max}(v_{\rm min})$ curve introduced in [18], where $t_{\rm max}$ is the time of maximum nuclear recoil rate. At the end of section 3.3, we also comment on the expected amplitude vs $v_{\rm min}$ and $t_{\rm max}$ vs $v_{\rm min}$ curves in the case of DM-nucleus magnetic dipole interactions. The timing information that we review in this section will then be used in the following two sections to assess the prospects for DM signal discovery and model selection with next-generation low-threshold detectors.

JCAP02(2022)022

3.1 Annual modulation amplitude

Since the vectors $\boldsymbol{V}_\oplus$ and $\hat{\boldsymbol{r}}_{\boldsymbol{s}}$ are periodic functions of t with period of one year, the rate of DM-nucleus scattering events, eq. (2.1), can be expanded in Fourier series around a reference time $t_0 > 0$,

$$\frac{\mathrm{d}R}{\mathrm{d}E_R} = A_0 + \sum_{n=1}^{\infty} A_n \cos n\omega(t - t_0) + \sum_{n=1}^{\infty} B_n \sin n\omega(t - t_0)\,, \tag{3.1}$$

where $\omega = 2\pi/\text{year}$ and for t_0 we choose the value of t that maximises the vector $\boldsymbol{v}_\odot + \boldsymbol{V}_\oplus$. The expansion coefficients A_0, A_n and B_n depend on the nuclear recoil energy or, equivalently, on $v_{\min}$. They also depend on the differential cross section for DM-nucleus scattering, which in turn depends on how DM couples to nuclei. If the DM velocity distribution in the Galactic reference frame is isotropic, then $B_n = 0$ [37]. Furthermore, when $f(\boldsymbol{v}, t)$ changes slowly over velocity variations of the order of $|\boldsymbol{V}_\oplus|$, then $A_0 \gg A_1 \gg A_{n\geq 2}$ [22]. The existence of this hierarchy is well-known in the case of the familiar spin-independent and spin-dependent interactions. In section 3.2, we show that it also applies to all DM-nucleon interactions considered in table 1. In the "single cosine approximation", all expansion coefficients in eq. (3.1) but A_0 and A_1 are set to zero. Within this approximation, the modulation amplitude, A_1, can be written as

$$A_1(v_{\min}) = \frac{1}{2}\left[\frac{\mathrm{d}R}{\mathrm{d}E_R}(v_{\min}, t_0) - \frac{\mathrm{d}R}{\mathrm{d}E_R}(v_{\min}, t_0 + \text{year}/2)\right]\,, \tag{3.2}$$

where we emphasised the dependence of the differential rate $\mathrm{d}R/\mathrm{d}E_R$ on $v_{\min}$ and the time of the year.

We now characterise the interactions in table 1 in terms of the predicted $A_1(v_{\min})$ curve. Since the dependence on v of the DM-nucleus scattering cross section determines the time-dependence of the nuclear recoil rate in eq. (2.1), we can restrict our analysis to the four representative interactions in eq. (2.7). For the latter, the four panels in figure 1 show A_1 as a function of $v_{\min}$. We set the DM mass to $m_\chi = 10\,\text{GeV}$ and one coupling constant at the time to $1/m_V^2$, where $m_V = 246\,\text{GeV}$. Each panel contains seven lines of different colours corresponding to distinct target materials: oxygen, aluminium, sodium, calcium, germanium, iodine and xenon. In our calculations, we take the isotopic abundance of the different elements into account. For the interactions $\mathcal{O}_1$ and $\mathcal{O}_{11}$ (top panels), the modulation amplitude changes sign for $v_{\min}$ around 200 km s^{-1}. This is consistent with having assumed $t_0 > 0$ and A_1 unconstrained. On the other hand, we could have assumed $A_1 > 0$ and t_0 unconstrained. This second convention would have implied a change of sign for t_0, i.e. an "inversion of phase", for $v_{\min} \sim 200$ km s^{-1}. For the interactions $\mathcal{O}_7$ and $\mathcal{O}_8$ (bottom panels) there is no inversion of phase, i.e. $A_1 > 0$ for every $v_{\min}$. Figure 1 also shows that for the $\mathcal{O}_1$, $\mathcal{O}_8$ and $\mathcal{O}_{11}$ interactions, the heavier the target the larger A_1. This is expected, as the corresponding scattering cross section depends on $W_M^{\tau\tau'}$, and, therefore, scales with the number of nucleons squared in the small momentum transfer limit. In contrast, for the spin-dependent $\mathcal{O}_7$ interaction, aluminium exhibits the largest modulation amplitude. Figure 2 shows A_1 as a function of $v_{\min}$ for the same interactions and targets as figure 1, but now for $m_\chi = 100\,\text{GeV}$. Changing the DM particle mass, our results remain qualitatively the same. Both figure 1 and figure 2 assume an exposure of 1 kg×day.

3.2 Higher-order harmonics

As we have seen in the previous subsection, the effective theory of DM-nucleon interactions predicts two families of modulation amplitude. In the first one, A_1 changes sign as a function

JCAP02(2022)022

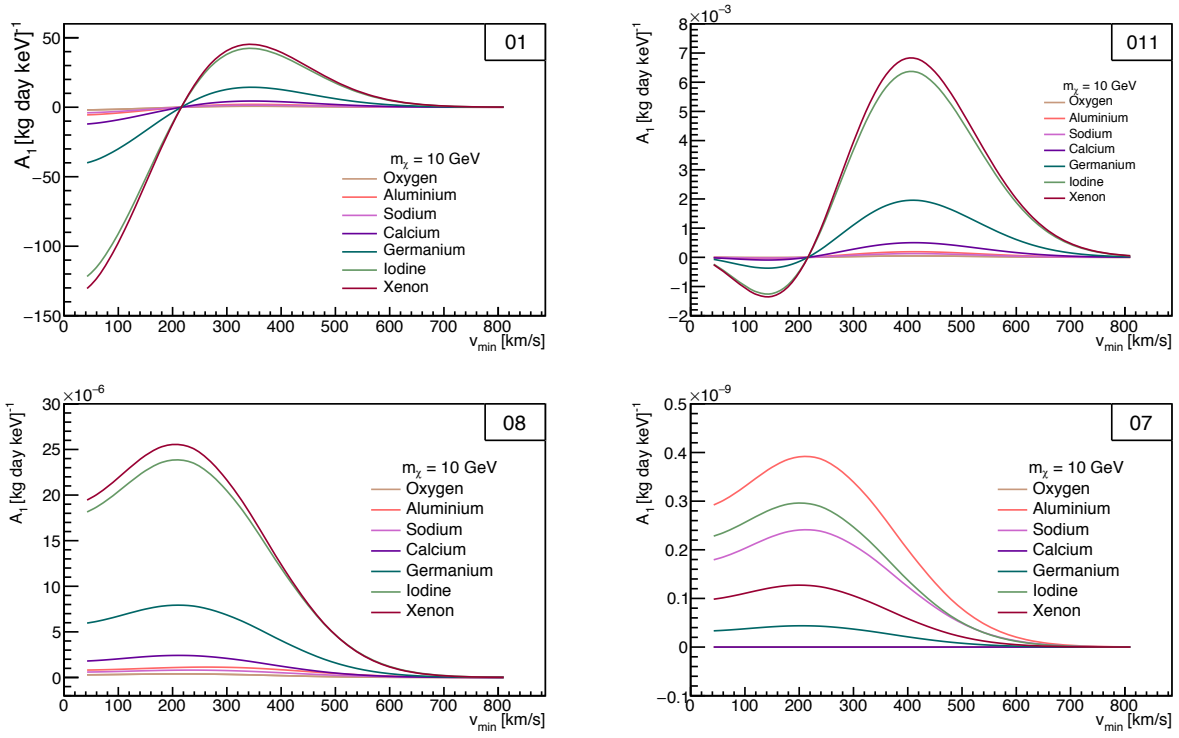

Figure 1. Modulation amplitude A_1 as a function of the minimum velocity $v_{\rm min}$ for m_χ=10 GeV and the four interactions $\mathcal{O}_1$, $\mathcal{O}_7$, $\mathcal{O}_8$ and $\mathcal{O}_{11}$. Different colours refers to distinct targets. For the interactions $\mathcal{O}_1$ and $\mathcal{O}_{11}$ (top panels), A_1 changes sign for $v_{\rm min}$ around 200 km s^{-1}. For the interactions $\mathcal{O}_7$ and $\mathcal{O}_8$ (bottom panels) $A_1 > 0$ for every $v_{\rm min}$. Here, we assume a positive reference time t_0 (see eq. (3.2)).

of $v_{\rm min}$. In the second one, $A_1 > 0$ for every $v_{\rm min}$. In this subsection we investigate the validity of the single cosine approximation, i.e. the hierarchy $A_0 \gg A_1 \gg A_{n\geq 2}$, for the two families of interactions. We focus on $\mathcal{O}_1$ and $\mathcal{O}_7$ as representatives of the first and second family, respectively.

Figure 3, left panel (right panel), shows the ratio $|A_1|/A_0$ ($|A_2|/|A_1|$) as a function of $v_{\rm min}$. Here, we consider two benchmark scenarios: 1) A DM particle with interactions of $\mathcal{O}_1$ type and mass of 50 GeV scattering on a xenon target (red, dot-dashed line). 2) A DM particle of mass 10 GeV interacting via the $\mathcal{O}_7$ interaction with an aluminium target (black, solid line). The red lines in figure 3 reproduce the results of [22], which we use to validate our calculations. The black lines correspond to results obtained here and of interest for a low-threshold detector operating Al_2O_3 crystals. The spike around 200 km s^{-1} in the $|A_1|/A_0$ curve for $\mathcal{O}_1$ reflects the change of sign of A_1 for this interaction. Similarly, the smooth $|A_1|/A_0$ curve associated with $\mathcal{O}_7$ follows from the constant sign of A_1 in this case. As far as the $|A_2|/|A_1|$ curve is concerned, we find two zeros at, respectively, 160-180 km s^{-1} and 500-540 km s^{-1} for the $\mathcal{O}_1$ interaction, and at 415-420 km s^{-1} and 690-700 km s^{-1} for the $\mathcal{O}_7$ interaction. Consequently, we conclude that the single cosine approximation is valid at all $v_{\rm min}$ for interactions where A_1 does not change sign, like $\mathcal{O}_7$. We also find that for interactions like $\mathcal{O}_1$ the single cosine approximation is valid at all $v_{\rm min}$ values but around 200 km s^{-1}, as expected. While we present our results focusing on two specific combinations of model parameters, it is important to stress that at a given $v_{\rm min}$, and for single interactions,

JCAP02(2022)022

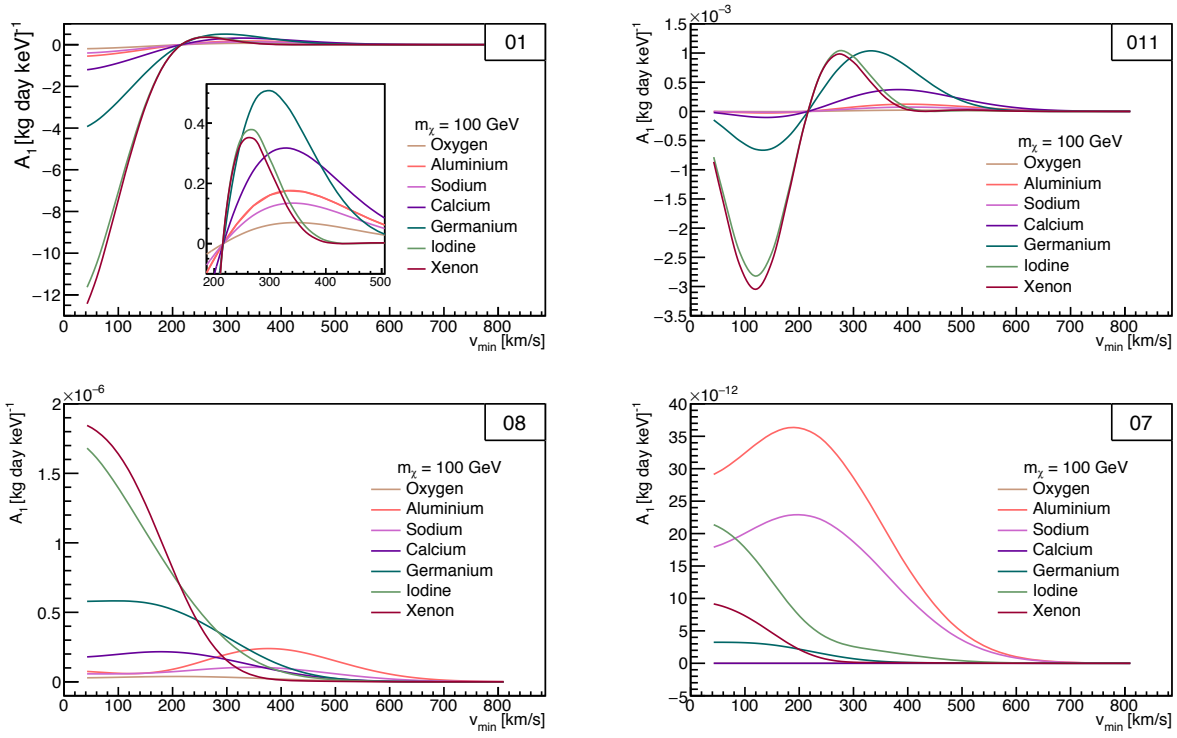

Figure 2. Same as figure 1, but now for $m_\chi = 100\,\text{GeV}$.

the ratios $|A_1|/A_0$ and $|A_2|/|A_1|$ do not depend on DM particle and target mass, as these are either reabsorbed in the definition of $v_{\min}$ or factored out in time-independent pre-factors; see eq. (3.5) below.[1]

3.3 Target dependence of the time of maximum rate

We now characterise the interactions in table 1 in terms of the predicted $t_{\max}(v_{\min})$ curve, extending previous results to target nuclei of interest for the CRESST experiments. We start by noticing that to evaluate the rate in eq. (2.1) with differential cross sections for DM-nucleus scattering given in eqs. (2.7) and (2.9), we have to compute one or two of the integrals,

$$\eta(v_{\min}, t) = \int_{v \geq v_{\min}} \mathrm{d}^3 v \, \frac{f(\boldsymbol{v}, t)}{v} \,, \tag{3.3}$$

$$\tilde{\eta}(v_{\min}, t) = \int_{v \geq v_{\min}} \mathrm{d}^3 v \, v f(\boldsymbol{v}, t) \,. \tag{3.4}$$

In terms of the $\eta(v_{\min}, t)$ and $\tilde{\eta}(v_{\min}, t)$ functions, the expected rate of nuclear recoils can be written as

$$\frac{\mathrm{d}R}{\mathrm{d}E_R} = \mathscr{A}(v_{\min}, m_T)\, \eta(v_{\min}, t) + \mathscr{B}(v_{\min}, m_T)\, \tilde{\eta}(v_{\min}, t) \,. \tag{3.5}$$

When $\mathscr{A}(v_{\min}, m_T) \neq 0$ and $\mathscr{B}(v_{\min}, m_T) = 0$, as in the case of the familiar spin-independent interaction, the time of maximum rate, $t_{\max}$, is entirely determined by $\eta(v_{\min}, t)$ and, as such,

[1] This is not exactly true for the category $\mathcal{O}_8$ ($\mathcal{O}_5$), since η and $\tilde{\eta}$ present different target dependent coefficients. However, figure 4 shows that the term proportional to $\tilde{\eta}$ dominates, therefore treating the ratios between higher order harmonics as independent from model parameters is a good approximation.

JCAP02(2022)022

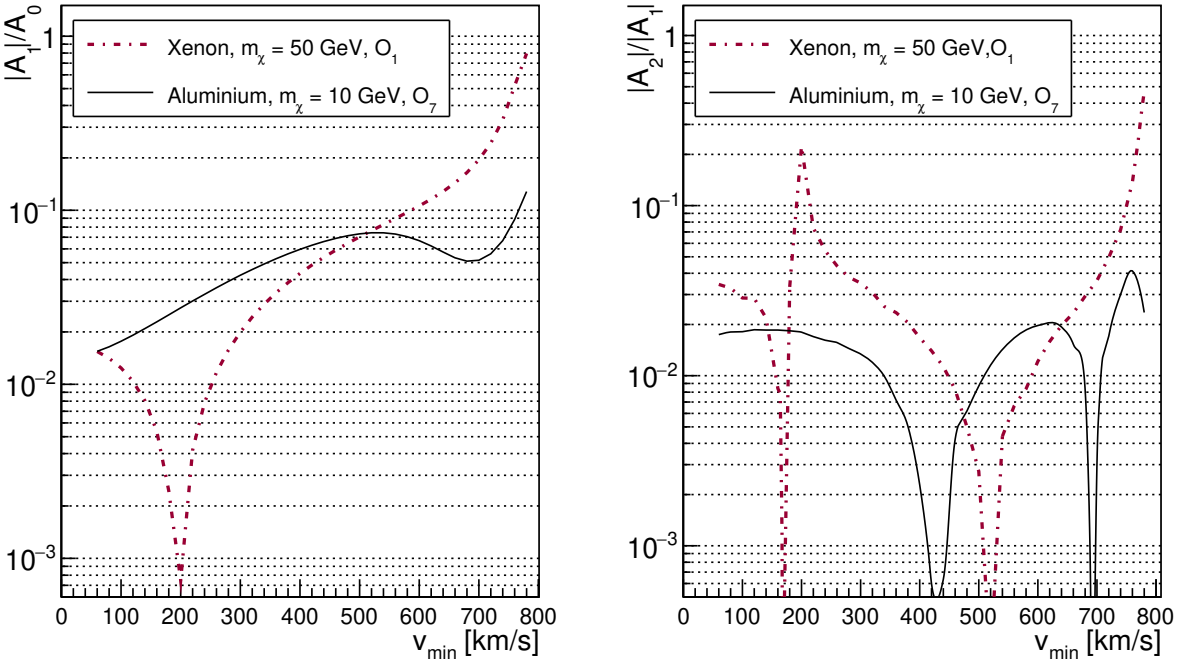

Figure 3. Ratios $|A_1|/A_0$ (left panel) and $|A_2|/|A_1|$ (right panel) as a function of $v_{\rm min}$. Red dot-dashed lines correspond to a DM particle of mass 50 GeV scattering on a xenon target via $\mathcal{O}_1$. Black solid lines refers to a DM particle of mass 10 GeV scattering on an aluminium target via $\mathcal{O}_7$. The hierarchy $A_0 \gg A_1 \gg A_2$ is valid at all $v_{\rm min}$ for interactions where A_1 does not change sign, like $\mathcal{O}_7$. It is valid at all $v_{\rm min}$ but around 200 km s^{-1} for interactions where A_1 changes sign around 200 km s^{-1}, like $\mathcal{O}_1$.

it is a universal, i.e. target-independent function of $v_{\rm min}$. The same applies to models where $\mathscr{B}(v_{\rm min}, m_T) \neq 0$ and $\mathscr{A}(v_{\rm min}, m_T) = 0$. However, if both $\mathscr{A}(v_{\rm min}, m_T)$ and $\mathscr{B}(v_{\rm min}, m_T)$ are different from zero and depend on m_T, and if the two terms in eq. (3.5) have comparable size, then the function $t_{\rm max}(v_{\rm min})$ can depend on the target the DM particle scatters on. In this latter case, there might be a range of $v_{\rm min}$ where the rate of DM-induced nuclear recoils observed by a multi-target detector depends on time via the superposition of two annual modulations of different phase. Therefore, it is important to understand whether the target dependence of $t_{\rm max}(v_{\rm min})$ is a generic feature of DM-nucleus interactions, or it can only occur in specific models. Here, we address this question within the effective theory of DM-nucleon interactions. First, we compute $t_{\rm max}(v_{\rm min})$ for single interactions in table 1. Then we focus on the specific linear combination of interaction operators corresponding to the DM magnetic dipole interaction model. This latter calculation extends the results of ref. [18] to aluminium, calcium and oxygen.

Inspection of eq. (2.7) and eq. (A.1) shows that $\mathscr{A}(v_{\rm min}, m_T)$ and $\mathscr{B}(v_{\rm min}, m_T)$ are simultaneously different from zero for the $\mathcal{O}_5$ and $\mathcal{O}_8$ interactions only. At the same time, by explicitly evaluating the $\mathscr{A}(v_{\rm min}, m_T)$ and $\mathscr{B}(v_{\rm min}, m_T)$ functions we find that in both cases the first term in eq. (3.5) always dominates over the second one. As a result, in models where DM couples to nuclei via one of the operators in table 1 at the time, $t_{\rm max}(v_{\rm min})$ is a universal, target-independent curve. We also find that all operators with differential cross section scaling like $a(q^2)/v^2$ and $e(q^2)v_{\rm min}^2/v^2$ predict a $t_{\rm max}(v_{\rm min})$ curve modulating from about January 1st at small $v_{\rm min}$ (when gravitational focusing is included) to June 1st at large $v_{\rm min}$. For

JCAP02(2022)022

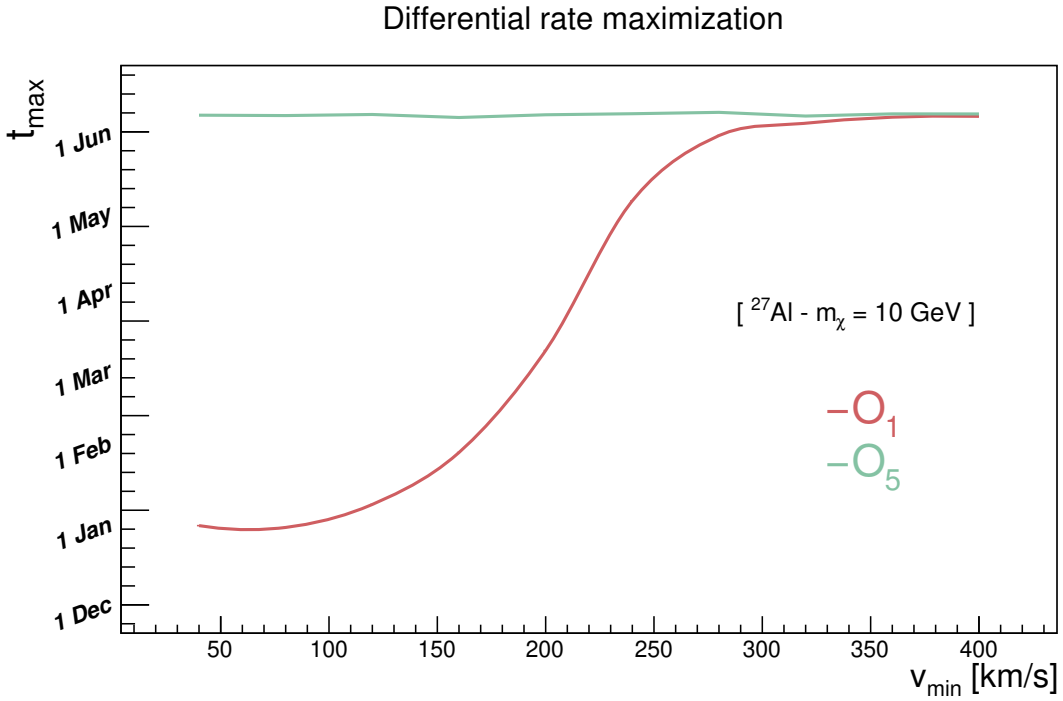

Figure 4. Time of maximum, $t_{\rm max}$, for the differential rate in eq. (2.1) as a function of $v_{\rm min}$ for the interactions $\mathcal{O}_1$ and $\mathcal{O}_5$. In the former case eq. (2.1) is proportional to the η function, in the latter to the $\tilde{\eta}$ function. In both cases, we assume aluminium as a target material and a DM particle mass of 10 GeV.

these interactions A_1 changes sign at small $v_{\rm min}$. For the remaining interactions, the curve $t_{\rm max}(v_{\rm min})$ is flat and A_1 has the same sign for all $v_{\rm min}$ values. Figure 4, left panel, illustrates our results on $t_{\rm max}(v_{\rm min})$ focusing on the $\mathcal{O}_1$ and $\mathcal{O}_5$ interactions.

Let us now focus on the DM magnetic dipole interaction model. Here, we extend the results of [18] to aluminium, calcium and oxygen, as these targets are of interest for CRESST detectors. Figure 5 shows the $t_{\rm max}(v_{\rm min})$ curve for calcium (top panels) and aluminium (bottom panels). The corresponding curve for oxygen is identical to the one associated with calcium. The right panels in figure 5 report differential nuclear recoil rates as a function of time for different values of $v_{\rm min}$ and, in the case of aluminium, for different DM particle masses. In the case of calcium, the curve $t_{\rm max}(v_{\rm min})$ is approximately flat, as the term proportional to the $\tilde{\eta}$ function in eq. (3.5) dominates over the term proportional to η. This is due to the fact that ^{16}O and ^{40}Ca have spin zero, which implies $W_{\Sigma'} = 0$. As a result, the surviving term in eq. (2.9) is proportional to W_M^{pp} for both the η and the $\tilde{\eta}$ contributions and the coefficient of $\tilde{\eta}$ is proportional to $1/v_{\rm min}^2$, which explains why the $\tilde{\eta}$ contribution dominates over the η one at small $v_{\rm min}$. In contrast, the curve $t_{\rm max}(v_{\rm min})$ has a minimum above 100 km s^{-1} in the case of aluminium. This arises from the interplay of the η and $\tilde{\eta}$ terms in eq. (3.5). However, this minimum is pronounced only for $m_\chi > 10$ GeV. Therefore, for magnetic dipole DM-nucleus interactions, aluminium, calcium and oxygen are characterised by the same, approximately flat $t_{\rm max}(v_{\rm min})$ curve for small m_χ values. On the other hand, for the familiar spin-independent interaction, the $t_{\rm max}(v_{\rm min})$ curve span a period of about five months. Consequently, it is reasonable to expect that timing information on the observed nuclear recoils can be used to discriminate spin-independent from magnetic dipole DM-nucleus interactions. Since the phenomenology of the two models significantly differs

JCAP02(2022)022

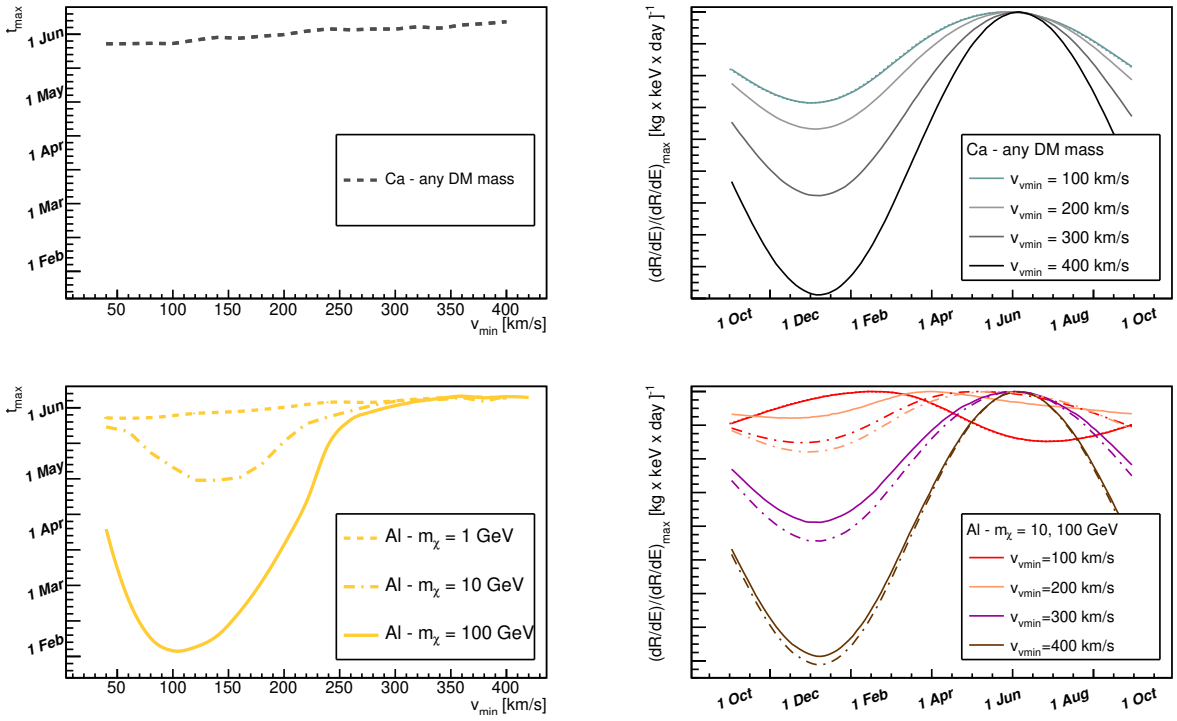

Figure 5. *Left panels.* Time of maximum differential rate of nuclear recoil events, $t_{\max}$, as a function of $v_{\min}$ for the DM magnetic dipole interaction model. The top panel assumes calcium as a target material, whereas the bottom panel refers to aluminium. *Right panels.* Differential rate at different $v_{\min}$ values for calcium (top panel) and aluminium (bottom panel). We set m_χ to the values in the legends.

in the small $v_{\min}$ limit, low-threshold experiments should then be optimal to discriminate between them. While we here focused on the DM magnetic dipole, we verified that the same conclusions apply to the anapole DM model, which predicts a similar $\mathrm{d}\sigma_T/\mathrm{d}E_R$.

4 Statistical framework

In this section, we introduce the statistical framework used to assess the prospects for DM signal discovery and model selection via timing (and energy) information in a low-threshold experiment. As anticipated, our goal is to determine whether a time dependent analysis can improve the sensitivity of CRESST in the presence of an unidentified background resembling the low-energy events recently reported by the CRESST collaboration. Here, we assume that n nuclear recoil events have been observed in a low-threshold detector. The data sample is distributed over a signal region, ΔS, that we divide into N bins. ΔS and the N bins are one-dimensional energy intervals, when we only analyse the energy spectrum of the nuclear recoils (1D analysis). They are two-dimensional, energy×time intervals, when we assume that timing information on the nuclear recoils is also accessible (2D analysis).

4.1 Signal discovery

Focusing on DM signal discovery, we compare the background-only hypothesis with an alternative, signal-plus-background hypothesis. In the background-only hypothesis the nuclear recoil events observed in the detector can be explained in terms of experimental backgrounds

JCAP02(2022)022

alone. In the signal-plus-background hypothesis, the observed events include a DM signal contribution. We model the energy spectrum of the background events by assuming that they are distributed in energy as the energy spectrum observed in CRESST-III, which presents an excess below 200 eV, as reported in [17] and described in the introduction. We also assume that the background events are homogeneously distributed in time. In our calculations, the number of background events, λ_b, in a pre-defined signal region ΔS is an input. We set λ_b to the desired value by varying the overall background normalisation, $\mathscr{B}$. This model for the experimental background is only taken as a reference for the order of magnitude of the expected background level, as the energy spectrum reported in [17] was observed using $CaWO_4$, whereas here we consider Al_2O_3 as target material. Specifically, for the experimental background we assume the energy spectrum [38],

$$\frac{\mathrm{d}N_b}{\mathrm{d}E_R} = \mathscr{B}\left(p_0 + p_1 E_R + p_2 e^{-E_R/p_3}\right) , \tag{4.1}$$

where we set p_0, p_1, p_2 and p_3 to the best fit values we found by fitting eq. (4.1) with $\mathscr{B} = 1$ to the data in [39] (file 'C3P1_DetA_full.dat'), namely: $p_0 = 28\,\mathrm{keV}^{-1}$, $p_1 = -0.8\,\mathrm{keV}^{-2}$, $p_2 = 19776\,\mathrm{keV}^{-1}$ and $p_3 = 0.0423\,\mathrm{keV}$. In the signal-plus-background hypothesis, we model the DM signal contribution in terms of spin-independent interactions. Specifically, we set the DM-nucleon scattering cross section, the proton to neutron coupling ratio and the DM particle mass to two benchmark set of values: 1) the best fit values found in a fit of the latest DAMA results [40], namely $\sigma_{\mathrm{SI}} = 2.67 \times 10^{-38}$ cm^2, $r = c_p/c_n = -0.76$ and $m_\chi = 11.17\,\mathrm{GeV}$, respectively [41]; and 2) $\sigma_{\mathrm{SI}} = 4 \times 10^{-42}$ cm^2, $r = c_p/c_n = 1$ and $m_\chi = 3\,\mathrm{GeV}$, respectively. The first benchmark allows us to test the relative impact of energy and timing information on the discovery of a signal resembling the one reported by DAMA. The second one corresponds to the 90% C.L. upper bound on the DM-nucleon scattering cross section reported by the DarkSide-50 collaboration for $m_\chi = 3\,\mathrm{GeV}$ [42]. Notice that $m_\chi = 3\,\mathrm{GeV}$ is the smallest DM mass that can induce values of v_{min} below 200 km s^{-1} for recoil energies below $\simeq 200\,\mathrm{eV}$, and that below 200 km s^{-1} the modulation amplitude changes sign in the case of spin-independent interactions.

Let us now denote by s_i the expected number of DM signal events in the i-th bin when the model parameters are set at one of the above benchmark points. The expected number of signal events in the signal region ΔS is hence $\lambda_s = \sum_i s_i$. Here, we adopt the notation of [43] and introduce the signal strength parameter, μ. For $\mu = 0$ there is no DM signal contribution to the observed nuclear recoil events, while for $\mu = 1$ the DM contribution to the i-th bin is s_i. Furthermore, we denote by b_i the expected number of background events in the i-th bin and introduce the parameter θ (see eq. (4.4)) to model the uncertainties in the background amplitude. Both in the 1D analysis and in the 2D analysis, we test the background-only hypothesis against the signal-plus-background hypothesis by means of the test statistic [43],

$$q_0 = \begin{cases} -2\ln\lambda & \hat{\mu} \geq 0 \\ 0 & \hat{\mu} < 0 \end{cases} \tag{4.2}$$

where

$$\lambda = \frac{\mathscr{L}(0, \hat{\hat{\theta}})}{\mathscr{L}(\hat{\mu}, \hat{\theta})} , \tag{4.3}$$

JCAP02(2022)022

and $\mathscr{L}(\mu,\theta)$ is the likelihood function,

$$\mathscr{L}(\mu,\theta)=\prod_{i=1}^{N}\frac{(\mu s_i+\theta b_i)^{n_i}}{n_i!}e^{-(\mu s_i+\theta b_i)}\,. \tag{4.4}$$

Here, $\hat{\hat{\theta}}$ is the value of θ that maximises $\mathscr{L}$ when $\mu=0$, while $(\hat{\mu},\hat{\theta})$ is the maximum likelihood estimator. We sample the total number of events (background plus signal) in the i-th bin, n_i, from a Poisson distribution of mean $\overline{\mu}s_i+\overline{\theta}b_i$, where $\overline{\mu}$ and $\overline{\theta}$ are the hypothesised values for μ and θ, respectively. For example, when sampling n_i under the background-only hypothesis, $\overline{\mu}=0$ and $\overline{\theta}=1$. When sampling n_i under the signal-plus-background hypothesis, $\overline{\mu}=1$ and $\overline{\theta}=1$. By repeatedly sampling n_i under the background-only hypothesis, we obtain the probability density function (pdf) $f(q_0|0)$. Sampling n_i under the signal-plus-background hypothesis we obtain the pdf $f(q_0|1)$. From $f(q_0|0)$ and $f(q_0|1)$, we obtain the p-value for signal discovery,

$$p=\int_{q_0^{\rm med}}^{\infty}\mathrm{d}q_0\,f(q_0|0)\,, \tag{4.5}$$

where $q_0^{\rm med}$ is the median of $f(q_0|1)$. In order to test the importance of the nuisance parameter θ, we also evaluate the p-value in eq. (4.5) for θ set to the constant value $\theta=\overline{\theta}=1$, so that $\hat{\hat{\theta}}=\hat{\theta}=1$.

4.2 Model selection

Focusing on DM model selection, we compare a "null-hypothesis" where DM couples to nuclei through the familiar spin-independent interaction, with an alternative hypothesis where DM couples to nuclei via a magnetic dipole moment. Within the null-hypothesis, we model the DM contribution to the observed nuclear recoils by assuming $m_\chi=3\,\mathrm{GeV}$, $r=c_p/c_n=1$ and $\sigma_{\rm SI}=4\times10^{-42}$ cm^2, as in one of the realisations of the signal-plus-background hypothesis considered in section 4.1. This set of parameters predicts 2.2 counts in an experimental setup consisting of an Al_2O_3 detector with an exposure of 23 g×year, when considering the interval [0.012−5.4] keV as energy window. Within the alternative hypothesis, we assume $m_\chi=3\,\mathrm{GeV}$ and couplings set to $\sigma_{\rm MD}\equiv4\alpha^2\lambda_\chi^2=4.72\times10^{-41}$ cm^2. This reference cross section value predicts 2.2 counts for the above experimental setup. Within both hypotheses, we model the experimental background as in section 4.1. Finally, we compare the two hypotheses by using the log-likelihood ratio test statistic,

$$q=-2\ln\widetilde{\lambda} \tag{4.6}$$

where

$$\widetilde{\lambda}=\frac{\mathscr{L}^{(0)}(\hat{\mu},\hat{\theta})}{\mathscr{L}^{(a)}(\hat{\mu},\hat{\theta})} \tag{4.7}$$

and

$$\begin{aligned}\mathscr{L}^{(0)}(\mu,\theta)&=\prod_{i=1}^{N}\frac{(\mu s_i^0+\theta b_i)^{n_i}}{n_i!}e^{-(\mu s_i^0+\theta b_i)}\,,\\ \mathscr{L}^{(a)}(\mu,\theta)&=\prod_{i=1}^{N}\frac{(\mu s_i^a+\theta b_i)^{n_i}}{n_i!}e^{-(\mu s_i^a+\theta b_i)}\,.\end{aligned} \tag{4.8}$$

JCAP02(2022)022

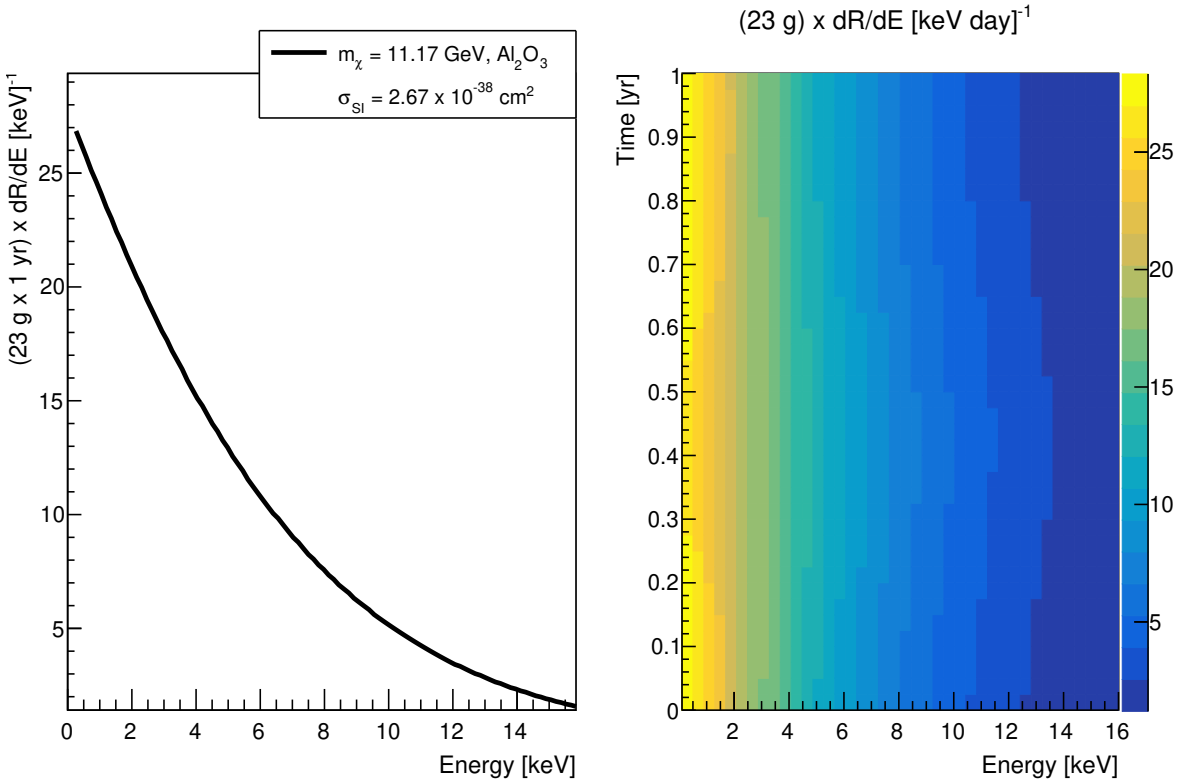

Figure 6. Predicted energy (left panel) and energy×time (right panel) distributions of DM-induced nuclear recoil events for our benchmark 1 scenario: $\sigma_{\rm SI} = 2.67 \times 10^{-38}$ cm^2, $r = c_p/c_n = -0.76$ and $m_\chi = 11.17\,$GeV.

Here, s_i^0 (s_i^a) is the number of expected signal events in the i-th bin under the null-hypothesis (alternative hypothesis). Importantly, n_i denotes the same dataset in both lines of eq. (4.8). Analogously to the case of DM signal discovery, we sample n_i from a Poisson distribution of mean $\overline{\mu}\,\overline{s}_i + \overline{\theta} b_i$. Sampling n_i under the null hypothesis, i.e. $\overline{\mu} = 1$, $\overline{\theta} = 1$ and $\overline{s}_i = s_i^0$, we obtain the pdf $f_0(q|1)$. Similarly, we obtain the pdf $f_a(q|1)$ when sampling n_i under the alternative hypothesis, i.e. $\overline{\mu} = 1$, $\overline{\theta} = 1$ and $\overline{s}_i = s_i^a$. Here, we quantify the ability of a low-threshold experiment to reject the null in favour of the alternative hypothesis in terms of the p-value,

$$p = \int_{q^{\rm med}}^{\infty} {\rm d}q\, f_0(q|1)\,, \tag{4.9}$$

where $q^{\rm med}$ is the median of the pdf $f_a(q|1)$.

5 Results

By applying the statistical methods of section 4 to the theoretical framework of section 2, we now report the result of our p-value calculations for DM signal discovery, section 5.1, and model selection, section 5.2. Here, we assume that the number of successes in observing a value of q (q_0) above $q^{\rm med}$ ($q_0^{\rm med}$) obeys a binomial distribution of variance $\sigma^2 = p\mathscr{N}(1-p)$, where $\mathscr{N}$ is the number of times we Monte Carlo generate the sample n_i. Consequently, the upper bound on the population error of our p-value estimates is given by $1/\sqrt{4\mathscr{N}}$. Since

JCAP02(2022)022

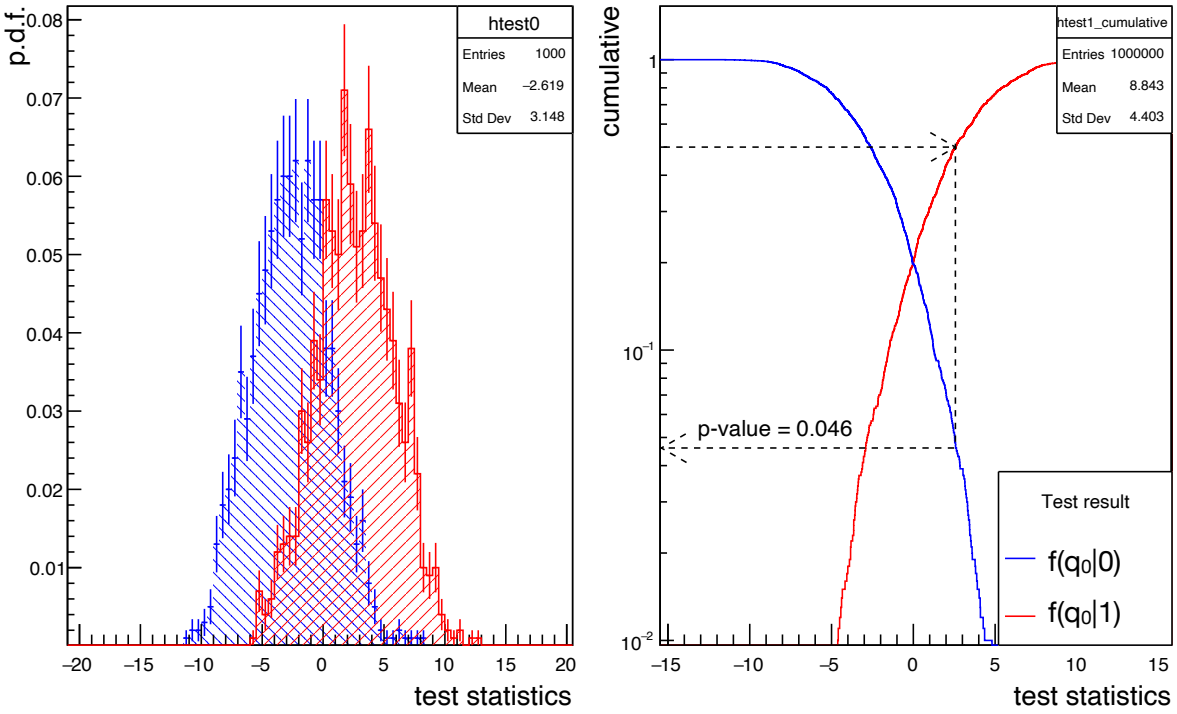

Figure 7. Probability density functions $f(q_0|0)$ and $f(q_0|1)$ (left panel) and associated cumulative probability density functions (right panel) for a simulation assuming no timing information, $\lambda_b = 10^3$ and our benchmark scenario 1. The p-value for DM discovery associated with this specific example is $p = 0.046$.

we choose $p = 0.1$ (i.e. 90% C.L.) as a reference p-value, we set $\mathscr{N}$ to 10^3. In the tables presented below, $p \simeq 0$ indicates that the result of our calculations is comparable or smaller than the associated error, $1/\sqrt{4\mathscr{N}} \simeq 0.016$.

5.1 Signal discovery

We start by testing the background-only hypothesis against the signal-plus-background hypothesis. We model the experimental background via eq. (4.1) and the DM contribution to the observed nuclear recoils in terms of spin-independent interactions. Here, we set the DM-nucleon scattering cross section, the proton to neutron coupling ratio and the DM particle mass to:

1. $\sigma_{\rm SI} = 2.67 \times 10^{-38}$ cm^2, $r = c_p/c_n = -0.76$ and $m_\chi = 11.17\,$GeV, respectively [41]. Furthermore, $\Delta S = [105\,\text{eV}, 16\,\text{keV}]$.

2. $\sigma_{\rm SI} = 4 \times 10^{-42}$ cm^2, $r_p/r_n = 1$ and $m_\chi = 3\,$GeV, respectively [42]. In addition, $\Delta S = [12\,\text{eV}, 5.4\,\text{keV}]$.

Our motivations for focusing on these two benchmarks have been discussed in section 3. The first one corresponds to the best fit to the latest DAMA results, the second one to the 90% C.L. upper limit on the DM-nucleon scattering cross section reported by the DarkSide-50 experiment. In both cases, we assume Al_2O_3 as target material and a minimum exposure of

JCAP02(2022)022

mass	time	λ_b	λ_s	N inter	p-value 1D	p-value 2D
23 g	1 yr	10^3	$\simeq 141$	10^3	$\simeq 0$	$\simeq 0$
〃	〃	10^4	〃	〃	0.046	0.045
〃	〃	10^5	〃	〃	0.284	0.247
2 x 23 g	〃	〃	$\simeq 283$	〃	0.161	0.163
3 x 23 g	〃	〃	$\simeq 424$	〃	0.055	0.077

Table 2. p-values for DM signal discovery in the case of a DAMA-like signal (benchmark scenario 1), known background and no nuisance parameters. The number of bins is set to 10 both for energy and time. The first and second column correspond to detector mass and time of data taking, respectively. The fifth column gives the number of independent test statistic evaluations in our Monte Carlo simulations. The p-values that we obtained in 1D (2D) analyses are reported in the sixth (seventh) column.

mass	time	λ_b	λ_s	N inter	p-value 1D	p-value 2D
23 g	158 days	500	$\simeq 69$	10^3	0.086	0.083
〃	1 yr	10^3	$\simeq 159$	〃	$\simeq 0$	$\simeq 0$
〃	〃	10^4	〃	〃	0.21	0.212
〃	〃	10^5	〃	〃	0.398	0.415
23 g	2 yr	$2 \cdot 10^3$	$\simeq 319$	〃	$\simeq 0$	$\simeq 0$
〃	〃	$2 \cdot 10^4$	〃	〃	0.127	0.14
〃	〃	$2 \cdot 10^5$	〃	〃	0.34	0.362

Table 3. Same as table 2, but now assuming an unknown background amplitude as a nuisance parameter.

23 g×158 days. In the 1D analyses nuclear recoils are distributed in 10 energy bins, while in the 2D analyses they are distributed in 10^2 energy×time bins. We test the results using both linear and logarithmic binning size. We use the test statistic in eq. (4.2).

5.1.1 Benchmark 1

Focusing on the first benchmark scenario, we now present our results on the ability of a low-threshold experiment to reject the background-only hypothesis. For this scenario, figure 6 shows the predicted energy (left panel) and energy×time (right panel) distributions of DM-induced nuclear recoil events. As expected from our analysis of $A_1(v_{\rm min})$ and $t_{\rm max}(v_{\rm min})$ in section 3, the 2D distribution peaks around December/January at small energies and in June at high energies.

Using the information contained in figure 6, we first test the ability of a low-threshold experiment to reject the background-only hypothesis when the background parameter θ is set to the constant value $\theta = \overline{\theta} = 1$. We will treat θ as a nuisance parameter later on. As an illustrative example of the geometric interpretation of the p-value for signal discovery in eq. (4.9), figure 7 shows the pdfs $f(q_0|0)$ and $f(q_0|1)$ and the associated cumulative pdfs for a simulation assuming no timing information, $\lambda_b = 10^3$, $\lambda_s \simeq 141$ and $\Delta S = [105\,\text{eV}, 16\,\text{keV}]$ as signal region. As reported in the legend, the p-value associated with this specific example is $p = 0.046$.

Table 2 extends the results in figure 7 and shows the p-values we find when θ is set to the constant value $\theta = \overline{\theta} = 1$ for different combinations of λ_b, the expected number of background

JCAP02(2022)022

mass	time	λ_s	λ_b	N iter	p-value 1D	p-value 2D
23 g	158 days	$\simeq 1$	500	10^3	0.436	0.482
230 g	〃	$\simeq 22$	10^4	〃	0.323	0.346
〃	2 yr	$\simeq 45$	$2 \cdot 10^4$	〃	0.223	0.263
〃	5 yr	$\simeq 112$	$5 \cdot 10^4$	〃	0.151	0.151
1 kg	〃	$\simeq 491$	〃	〃	$\simeq 0$	$\simeq 0$
〃	〃	〃	$5 \cdot 10^5$	〃	0.065	0.094

Table 4. Same as table 3, but now modelling the DM-nucleon interaction as in our benchmark 2 scenario.

JCAP02(2022)022

events, and experimental exposures. More specifically, we consider values of λ_b ranging from 10^3 to 10^5 and experimental exposures varying from 23 g×year to 3×23 g×year. Importantly, in table 2 we report p-values for signal discovery that we obtain when timing information is taken into account (2D analysis) and when timing information is not available (1D analysis). As one can see from table 2, timing information has a marginal impact on the ability of a low-threshold experiment to reject the background-only hypothesis when the background events are modelled as in eq. (4.1) and the observed DM signal resembles the one reported by DAMA.

We now present our results on the ability of a low-threshold experiment to reject the background-only hypothesis when the background parameter θ is considered as a nuisance parameter. Table 3 shows the p-values for signal discovery that we find in simulations where λ_b varies from 500 to 2×10^5, the experimental exposure varies from 23 g×158 days (corresponding to the exposure reached in the CRESST-III analysis [17]) to 23 g×2 years and θ is treated as a nuisance parameter. As in the case of table 2, table 3 shows the results we find when timing information on the observed nuclear recoils is taken into account, and when the latter is not available. Comparing table 2 with 3, one can see that in all cases the p-values we find when θ is a nuisance parameters are larger than when the experimental background is assumed to be known. This result is expected, as the Neyman-Pearson lemma (see [43] and references therein) states that the likelihood ratio in eq. (4.2) for $\theta = \overline{\theta} = 1$ is the test statistic with the highest significance power, i.e. the highest probability of rejecting the background-only hypothesis if the background-plus-signal hypothesis is true. Table 3 also shows that timing information has a marginal impact on the ability of a low-threshold experiment to reject the background-only hypothesis in favour of benchmark 1 in the case of an unknown background amplitude.

5.1.2 Benchmark 2

Now we turn our attention to the second benchmark scenario considered in this investigation, where $\sigma_{\rm SI} = 4 \times 10^{-42}$ cm^2, $r = c_p/c_n = 1$ and $m_\chi = 3\,$GeV. Focusing on this second scenario, below we present our results on the ability of a low-threshold experiment to reject the background-only hypothesis. We only consider the case of a background of unknown amplitude and treat θ as a nuisance parameter. Table 4 shows the p-values for signal discovery that we find comparing the background-only hypothesis with a DM signal model corresponding to our benchmark 2. In our analysis of benchmark 2, we let the number of background events, λ_b, vary from 500 to 5×10^5 and consider experimental exposures varying from 23 g×158 days to 1 kg×5 years.

Our results for benchmark 2 are summarised in table 4. In the 1D analysis, the p-values we obtain range from about 0.44, for $\lambda_b = 500$ and an exposure of 23 g×158 days, to about 0.06, for $\lambda_b = 5 \times 10^5$ and an exposure of 1 kg×5 years. Consistently with benchmark 2 being about two orders of magnitude below the current CRESST-III exclusion limit on $\sigma_{\rm SI}$ for $m_\chi = 3\,\text{GeV}$, we find that the CRESST experiment must operate with an exposure about 100 larger than the current one, i.e. 23 g×158 days, in order to achieve a 90% C.L. discovery of a DM model like benchmark 2. Remarkably, in all cases investigated here we find comparable p-values in the 1D analysis and in the 2D analysis, where timing information is taken into account. We therefore conclude that timing information has a marginal impact on the ability of a low-threshold experiment to reject the background-only hypothesis in favour of benchmark 2. These results have been verified to be stable both using the linear and the logarithmic distributed binning size.

5.2 Model selection

We conclude this section by presenting our results on the ability of a low-threshold experiment to reject spin-independent in favour of magnetic dipole DM-nucleon interactions. We refer to the former case as "null-hypothesis" and to the latter as "alternative hypothesis". As anticipated, we model the null-hypothesis by assuming $m_\chi = 3\,\text{GeV}$, $r_p/r_n = 1$ and $\sigma_{\rm SI} = 4 \times 10^{-42}$ cm^2. This set of parameters predicts 2.2 counts in the $[0.012 - 5.4]\,\text{keV}$ energy window for an Al_2O_3 detector with an exposure of 23 g×year. We model the alternative hypothesis by assuming $m_\chi = 3\,\text{GeV}$ and a cross section $\sigma_{\rm MD} \equiv 4\alpha\lambda_\chi^2 = 4.72 \times 10^{-41}$ cm^2. Consistently, this reference cross section value produces 2.2 counts in the same Al_2O_3 detector and energy window.

Table 5 shows the p-values we find when comparing null and alternative hypotheses. In this investigation, we consider experimental exposures ranging from 23 g×158 days to 1 kg×5 years, and λ_b varying from 10^3 to 2×10^4. We report both p-values for the 1D analysis and p-values for the 2D analysis, where timing information is taken into account. In all cases, we treat the background parameter θ as a nuisance parameter. The information in table 5 is two-fold. On the one hand we find that a 2D-analysis based on the energy and time distribution of the event rate produces more significant results with respect to the 1D analysis, at equal exposure. While previous results do not depend on the linear or logarithmic binning method, the different significance of the 2D and 1D analyses in this case strictly depends on the better accuracy of the logarithmic method. On the other hand, our results show that a 90% C.L. rejection of spin-independent interactions in favour of a DM magnetic dipole coupling is feasible at the CRESST experiment with an exposure of 460 g×year and 2×10^3 background events.

6 Summary and conclusions

We assessed the prospects for DM signal discovery and model selection via timing information in a low-threshold experiment. In all calculations, we assumed a time-independent experimental background with an energy spectrum resembling the one of the low-energy events observed in [17]. We focused on Al_2O_3 as a detector material, as it is composed of two relatively light elements (oxygen and aluminium) and showed very good performances, with energy thresholds as low as 19 eV [1].

As a preparatory step, we critically reviewed the timing information that is available to low-threshold multi-target experiments, focusing on interaction-dependent features, such as

JCAP02(2022)022

mass	time	λ_b	λ_s	N inter	p-value 1D	p-value 2D
23 g	1 yr	10^3	$\simeq 2.2$	10^3	0.486	0.442
230 g	2 yr	$2 \cdot 10^3$	$\simeq 44$	$''$	0.107	0.065
$''$	5 yr	$5 \cdot 10^3$	$\simeq 110$	$''$	0.024	0.005 ($\simeq 0$)
1 kg	$''$	$2 \cdot 10^4$	$\simeq 478$	$''$	$\simeq 0$	$\simeq 0$

Table 5. p-values for rejecting spin-independent interactions with $m_\chi = 3\,\text{GeV}$ and $\sigma_{\text{SI}} = 4 \times 10^{-42}$ cm^2 in favour of a magnetic dipole coupling producing the same number of events in $\Delta S = [12\,\text{eV}, 5.4\,\text{keV}]$. We report results with and without timing information, obtained with logarithmic binning. The notation is the same as in previous tables.

the shape of the $t_{\text{max}}(v_{\text{min}})$ curve, which can depend on the target material. We also explored the significance of higher-order harmonics in a Fourier series expansion of the predicted nuclear recoil rate. We discussed these aspects within the general non-relativistic effective theory of DM-nucleon interactions, and for specific interaction models, such as the DM magnetic dipole coupling.

Focusing on DM signal discovery, we compared a background-only hypothesis with an alternative, background-plus-signal hypothesis. Here, we modelled the interaction between DM and nuclei in terms of spin-independent interactions and considered two benchmark scenarios separately. The first scenario corresponds to the best fit mass and couplings to the latest DAMA/LIBRA results. The second one corresponds to the 90% C.L upper limit on the spin-independent DM-nucleon scattering cross section reported by DarkSide-50 for a DM particle mass of 3 GeV. Focusing on DM model selection, we compared a "null-hypothesis" where DM couples to nuclei through the familiar spin-independent interaction (and parameters as in the second scenario described above) with an alternative hypothesis where DM couples to nuclei via a magnetic dipole moment. We presented our results on the ability of a low-threshold experiment to discover a signal above a background resembling the excess found in the CRESST-III energy spectrum, or reject the spin-independent interaction in favour of a magnetic dipole coupling in terms of p-values, that we list in tables 2, 3, 4 and 5. Importantly, we performed our p-value calculations under two different assumptions: 1) Taking timing information into account. 2) Assuming that the latter is not available.

Remarkably, we found that while timing information has a marginal impact on the potential for DM signal discover, it can be beneficial for model selection in a low-threshold experiment. This conclusion arises from the fact that the difference between the assumed background and signal energy spectra is significantly larger than the difference between the energy spectra resulting from spin-independent and magnetic dipole interactions. This applies to all cases studied here and reported in tables 2, 3, 4 and 5. On the one hand, our results indicate that for this class of experiments it might not be worth tackling the challenge of operating cryogenic detectors under stable conditions for long periods, until the goal remains observing the first dark matter signal. On the other hand, if cryogenic experiments undertake such an effort, in case of detection of a positive dark matter signal, the timing information could provide more reliable results on the dark matter nature. For example, we found that the p-value for rejecting spin-independent interactions in favour of a magnetic dipole coupling is of about 0.1 when the exposure is 460 g×year, while about 0.06 if timing information is taken into accout. Our simulations are limited to at most 5 years of data taking, specific benchmarks and to the assumption of a background constant in time; it should

JCAP02(2022)022

be considered as a starting point towards further, refined analyses of the impact of timing information on the performance of future low-threshold experiments.

In addition, our results also show that for the set of model parameters considered here a 90% C.L. rejection of spin-independent interactions in favour of a magnetic dipole coupling is feasible with an upgrade of the CRESST experiment [2], where timing information is not still available; see table 5, second row. In order to consolidate our findings, we compared spin-independent and magnetic dipole interactions under the assumption of a detector efficiency below 100%. Specifically, in our likelihood analysis we multiplied the expected number of signal events in each bin, s_i, by a detector efficiency sampled from a uniform distribution in the 50% - 70% range. For an exposure of 1 kg×2 years and a background level of 5×10^3, we found a p-value for model selection of 0.072. As expected, the experimental sensitivity diminishes when detector efficiency is taken into account. At the same time, we found that a 90% C.L. rejection of spin-independent interactions in favour of a magnetic dipole coupling is feasible at a CRESST-III experiment, even when the detector efficiency is below 100%.

Acknowledgments

This work has been performed within a double doctoral degree agreement between Chalmers University and Technology and the Gran Sasso Science Institute. The authors thank, Federica Petricca, Paolo Gorla, Karoline Schäffner and Francesco Vissani for stimulating and supporting the implementation of the agreement between the two institutes, and Florian Reindl and the CRESST Collaboration for the many valuable discussions and suggestions which inspired the research contained in this work. RC acknowledges support from an individual research grant from the Swedish Research Council, dnr. 2018-05029. The results presented here made use of the computer programmes `Wolfram Mathematica` [44] and `DMFormFactor` [36].

A DM response functions

$$
\begin{aligned}
R_M^{\tau\tau'}\left(v_T^{\perp 2}, \frac{q^2}{m_N^2}\right) &= c_1^\tau c_1^{\tau'} + \frac{J_\chi(J_\chi+1)}{3}\left[\frac{q^2}{m_N^2} v_T^{\perp 2} c_5^\tau c_5^{\tau'} + v_T^{\perp 2} c_8^\tau c_8^{\tau'} + \frac{q^2}{m_N^2} c_{11}^\tau c_{11}^{\tau'}\right] \\
R_{\Phi''}^{\tau\tau'}\left(v_T^{\perp 2}, \frac{q^2}{m_N^2}\right) &= \frac{q^2}{4m_N^2} c_3^\tau c_3^{\tau'} + \frac{J_\chi(J_\chi+1)}{12}\left(c_{12}^\tau - \frac{q^2}{m_N^2} c_{15}^\tau\right)\left(c_{12}^{\tau'} - \frac{q^2}{m_N^2} c_{15}^{\tau'}\right) \\
R_{\Phi''M}^{\tau\tau'}\left(v_T^{\perp 2}, \frac{q^2}{m_N^2}\right) &= c_3^\tau c_1^{\tau'} + \frac{J_\chi(J_\chi+1)}{3}\left(c_{12}^\tau - \frac{q^2}{m_N^2} c_{15}^\tau\right) c_{11}^{\tau'} \\
R_{\tilde{\Phi}'}^{\tau\tau'}\left(v_T^{\perp 2}, \frac{q^2}{m_N^2}\right) &= \frac{J_\chi(J_\chi+1)}{12}\left[c_{12}^\tau c_{12}^{\tau'} + \frac{q^2}{m_N^2} c_{13}^\tau c_{13}^{\tau'}\right] \\
R_{\Sigma''}^{\tau\tau'}\left(v_T^{\perp 2}, \frac{q^2}{m_N^2}\right) &= \frac{q^2}{4m_N^2} c_{10}^\tau c_{10}^{\tau'} + \frac{J_\chi(J_\chi+1)}{12}\left[c_4^\tau c_4^{\tau'} + \frac{q^2}{m_N^2}(c_4^\tau c_6^{\tau'} + c_6^\tau c_4^{\tau'}) + \frac{q^4}{m_N^4} c_6^\tau c_6^{\tau'}\right. \\
&\qquad \left. + v_T^{\perp 2} c_{12}^\tau c_{12}^{\tau'} + \frac{q^2}{m_N^2} v_T^{\perp 2} c_{13}^\tau c_{13}^{\tau'}\right] \\
R_{\Sigma'}^{\tau\tau'}\left(v_T^{\perp 2}, \frac{q^2}{m_N^2}\right) &= \frac{1}{8}\left[\frac{q^2}{m_N^2} v_T^{\perp 2} c_3^\tau c_3^{\tau'} + v_T^{\perp 2} c_7^\tau c_7^{\tau'}\right] \frac{J_\chi(J_\chi+1)}{12}\left[c_4^\tau c_4^{\tau'} + \frac{q^2}{m_N^2} c_9^\tau c_9^{\tau'}\right. \\
&\qquad \left. + \frac{v_T^{\perp 2}}{2}\left(c_{12}^\tau - \frac{q^2}{m_N^2} c_{15}^\tau\right)\left(c_{12}^{\tau'} - \frac{q^2}{m_N^2} c_{15}^{\tau\prime}\right) + \frac{q^2}{2m_N^2} v_T^{\perp 2} c_{14}^\tau c_{14}^{\tau'}\right]
\end{aligned}
$$

JCAP02(2022)022

$$R_{\Delta}^{\tau\tau'}\left(v_T^{\perp 2},\frac{q^2}{m_N^2}\right)=\frac{J_\chi(J_\chi+1)}{3}\left[\frac{q^2}{m_N^2}c_5^\tau c_5^{\tau'}+c_8^\tau c_8^{\tau'}\right]$$
$$R_{\Delta\Sigma'}^{\tau\tau'}\left(v_T^{\perp 2},\frac{q^2}{m_N^2}\right)=\frac{J_\chi(J_\chi+1)}{3}\left[c_5^\tau c_4^{\tau'}-c_8^\tau c_9^{\tau'}\right], \tag{A.1}$$

where J_χ is the DM particle spin. In all numerical application in the work, for DM we assume $J_\chi = 1/2$.

References

[1] CRESST collaboration, *Results on MeV-scale dark matter from a gram-scale cryogenic calorimeter operated above ground*, *Eur. Phys. J. C* **77** (2017) 637 [arXiv:1707.06749] [INSPIRE].

[2] CRESST collaboration, *Probing low WIMP masses with the next generation of CRESST detector*, arXiv:1503.08065 [INSPIRE].

[3] G. Bertone and D. Hooper, *History of dark matter*, *Rev. Mod. Phys.* **90** (2018) 045002 [arXiv:1605.04909] [INSPIRE].

[4] A. Drukier and L. Stodolsky, *Principles and applications of a neutral current detector for neutrino physics and astronomy*, *Phys. Rev. D* **30** (1984) 2295 [INSPIRE].

[5] M.W. Goodman and E. Witten, *Detectability of certain dark matter candidates*, *Phys. Rev. D* **31** (1985) 3059 [INSPIRE].

[6] T. Marrodán Undagoitia and L. Rauch, *Dark matter direct-detection experiments*, *J. Phys. G* **43** (2016) 013001 [arXiv:1509.08767] [INSPIRE].

[7] Particle Data Group collaboration, *Review of particle physics*, *PTEP* **2020** (2020) 083C01 [INSPIRE].

[8] R. Trotta, R. Ruiz de Austri and L. Roszkowski, *Prospects for direct dark matter detection in the constrained MSSM*, *New Astron. Rev.* **51** (2007) 316 [astro-ph/0609126] [INSPIRE].

[9] R. Trotta, R. Ruiz de Austri and L. Roszkowski, *Direct dark matter detection around the corner? Prospects in the constrained MSSM*, *J. Phys. Conf. Ser.* **60** (2007) 259 [INSPIRE].

[10] D.G. Cerdeno, T. Kobayashi and C. Muñoz, *Prospects for the direct detection of neutralino dark matter in orbifold scenarios*, *JHEP* **01** (2008) 009 [arXiv:0709.0858] [INSPIRE].

[11] D.S.M. Alves, M. Lisanti and J.G. Wacker, *Poker face of inelastic dark matter: prospects at upcoming direct detection experiments*, *Phys. Rev. D* **82** (2010) 031901 [arXiv:1005.5421] [INSPIRE].

[12] R. Catena, *Prospects for direct detection of dark matter in an effective theory approach*, *JCAP* **07** (2014) 055 [arXiv:1406.0524] [INSPIRE].

[13] E. Del Nobile, G.B. Gelmini and S.J. Witte, *Prospects for detection of target-dependent annual modulation in direct dark matter searches*, *JCAP* **02** (2016) 009 [arXiv:1512.03961] [INSPIRE].

[14] P. Sandick, K. Sinha and F. Teng, *Simplified dark matter models with charged mediators: prospects for direct detection*, *JHEP* **10** (2016) 018 [arXiv:1608.00642] [INSPIRE].

[15] B.J. Kavanagh, F.S. Queiroz, W. Rodejohann and C.E. Yaguna, *Prospects for determining the particle/antiparticle nature of WIMP dark matter with direct detection experiments*, *JHEP* **10** (2017) 059 [arXiv:1706.07819] [INSPIRE].

[16] S.J. Witte, V. Gluscevic and S.D. McDermott, *Prospects for distinguishing dark matter models using annual modulation*, *JCAP* **02** (2017) 044 [arXiv:1612.07808] [INSPIRE].

JCAP02(2022)022

[17] CRESST collaboration, *First results from the CRESST-III low-mass dark matter program*, *Phys. Rev. D* **100** (2019) 102002 [arXiv:1904.00498] [INSPIRE].

[18] E. Del Nobile, G.B. Gelmini and S.J. Witte, *Target dependence of the annual modulation in direct dark matter searches*, *Phys. Rev. D* **91** (2015) 121302 [arXiv:1504.06772] [INSPIRE].

[19] M.S. Alenazi and P. Gondolo, *Phase-space distribution of unbound dark matter near the Sun*, *Phys. Rev. D* **74** (2006) 083518 [astro-ph/0608390] [INSPIRE].

[20] S.K. Lee, M. Lisanti, A.H.G. Peter and B.R. Safdi, *Effect of gravitational focusing on annual modulation in dark-matter direct-detection experiments*, *Phys. Rev. Lett.* **112** (2014) 011301 [arXiv:1308.1953] [INSPIRE].

[21] C. McCabe, *The earth's velocity for direct detection experiments*, *JCAP* **02** (2014) 027 [arXiv:1312.1355] [INSPIRE].

[22] S.K. Lee, M. Lisanti and B.R. Safdi, *Dark-matter harmonics beyond annual modulation*, *JCAP* **11** (2013) 033 [arXiv:1307.5323] [INSPIRE].

[23] J. Fan, M. Reece and L.-T. Wang, *Non-relativistic effective theory of dark matter direct detection*, *JCAP* **11** (2010) 042 [arXiv:1008.1591] [INSPIRE].

[24] A.L. Fitzpatrick, W. Haxton, E. Katz, N. Lubbers and Y. Xu, *The effective field theory of dark matter direct detection*, *JCAP* **02** (2013) 004 [arXiv:1203.3542] [INSPIRE].

[25] P. Gondolo, S. Kang, S. Scopel and G. Tomar, *Effective theory of nuclear scattering for a WIMP of arbitrary spin*, *Phys. Rev. D* **104** (2021) 063017 [arXiv:2008.05120] [INSPIRE].

[26] D. Gazda, R. Catena and C. Forssén, *Ab initio nuclear response functions for dark matter searches*, *Phys. Rev. D* **95** (2017) 103011 [arXiv:1612.09165] [INSPIRE].

[27] M. Hoferichter, P. Klos and A. Schwenk, *Chiral power counting of one- and two-body currents in direct detection of dark matter*, *Phys. Lett. B* **746** (2015) 410 [arXiv:1503.04811] [INSPIRE].

[28] F. Bishara, J. Brod, B. Grinstein and J. Zupan, *Chiral effective theory of dark matter direct detection*, *JCAP* **02** (2017) 009 [arXiv:1611.00368] [INSPIRE].

[29] R. Catena, J. Conrad and M.B. Krauss, *Compatibility of a dark matter discovery at XENONnT or LZ with the WIMP thermal production mechanism*, *Phys. Rev. D* **97** (2018) 103002 [arXiv:1712.07969] [INSPIRE].

[30] S. Baum, R. Catena, J. Conrad, K. Freese and M.B. Krauss, *Determining dark matter properties with a XENONnT/LZ signal and LHC run* 3 *monojet searches*, *Phys. Rev. D* **97** (2018) 083002 [arXiv:1709.06051] [INSPIRE].

[31] S. Baum, R. Catena and M.B. Krauss, *Impact of a XENONnT signal on LHC dijet searches*, *JHEP* **07** (2019) 015 [arXiv:1812.01594] [INSPIRE].

[32] S. Baum, R. Catena and M.B. Krauss, *Constraints on new scalar and vector mediators from LHC dijet searches*, *J. Phys. G* **47** (2020) 055001 [arXiv:1812.01585] [INSPIRE].

[33] B.J. Kavanagh, P. Panci and R. Ziegler, *Faint light from dark matter: classifying and constraining dark matter-photon effective operators*, *JHEP* **04** (2019) 089 [arXiv:1810.00033] [INSPIRE].

[34] M.I. Gresham and K.M. Zurek, *Effect of nuclear response functions in dark matter direct detection*, *Phys. Rev. D* **89** (2014) 123521 [arXiv:1401.3739] [INSPIRE].

[35] R. Catena and B. Schwabe, *Form factors for dark matter capture by the Sun in effective theories*, *JCAP* **04** (2015) 042 [arXiv:1501.03729] [INSPIRE].

[36] N. Anand, A.L. Fitzpatrick and W.C. Haxton, *Weakly interacting massive particle-nucleus elastic scattering response*, *Phys. Rev. C* **89** (2014) 065501 [arXiv:1308.6288] [INSPIRE].

JCAP02(2022)022

[37] K. Freese, M. Lisanti and C. Savage, *Colloquium: annual modulation of dark matter*, *Rev. Mod. Phys.* **85** (2013) 1561 [arXiv:1209.3339] [INSPIRE].

[38] D. Schmiedmayer, *Calculation of dark-matter exclusions-limits using a maximum likelihood approach*, master's thesis, Technische Universität Wien, Vienna, Austria (2019).

[39] CRESST collaboration, *Description of CRESST-III data*, arXiv:1905.07335 [INSPIRE].

[40] R. Bernabei et al., *First model independent results from DAMA/LIBRA-phase2*, *Nucl. Phys. Atom. Energy* **19** (2018) 307 [arXiv:1805.10486] [INSPIRE].

[41] S. Kang, S. Scopel, G. Tomar and J.-H. Yoon, *DAMA/LIBRA-phase2 in WIMP effective models*, *JCAP* **07** (2018) 016 [arXiv:1804.07528] [INSPIRE].

[42] DarkSide collaboration, *Low-mass dark matter search with the DarkSide-50 experiment*, *Phys. Rev. Lett.* **121** (2018) 081307 [arXiv:1802.06994] [INSPIRE].

[43] G. Cowan, K. Cranmer, E. Gross and O. Vitells, *Asymptotic formulae for likelihood-based tests of new physics*, *Eur. Phys. J. C* **71** (2011) 1554 [*Erratum ibid.* **73** (2013) 2501] [arXiv:1007.1727] [INSPIRE].

[44] Wolfram Research Inc., *Mathematica* v12.0, https://www.wolfram.com/mathematica/, U.S.A. (2019).

JCAP02(2022)022